Progress In Electromagnetics Research M, Vol. 46, 101–112, 2016

Target Detection in Low Grazing Angle with OFDM MIMO Radar

Yang Xia*, Zhiyong Song, Zaiqi Lu, and Qiang Fu

Abstract—In low grazing angle scenario, target detection performance is seriously deteriorated due to multipath effect. This paper deals with moving target detection in low grazing angle with orthogonal frequency division multiplexing (OFDM) multi-input multi-output (MIMO) radar. We show that the detection performance can be improved through utilizing the multipath effect. Realistic physical and statistical effects such as refraction of the lower atmosphere and the Earth's curvature are incorporated into the multipath propagation model. Then, we derive a generalized likelihood ratio test (GLRT) detector by taking advantage of the frequency diversity of OFDM and MIMO configuration. Based on the fact that the target responses resonate at different frequencies and statistical characteristics of the test, we propose an algorithm which adaptively allocates the transmitted energy to improve the detection performance. The effectiveness of the GLRT detector as well as the adaptive design method is demonstrated via numerical examples.

1. INTRODUCTION

Target detection and tracking in low grazing angle scenario is one of the most challenging problems in radar fields [1], where multipath effect is the main problem. The received signal is the coherent sum of direct and indirect signals. Amplitudes of the total received signals fluctuate due to the random phase variation of indirect signals (related to the path difference, wavelength and reflected surface [2]), which may seriously deteriorate the detection and tracking performances.

Traditional methods dealing with multipath effect are to regard it as clutter component, thus suppress it (e.g., see [3–6]). On the other hand, indirect signals also contain target energy, and the detection or tracking performance may be enhanced if energy from the indirect path is accumulated. A large amount of salient work has been done on this aspect. The prior knowledge on the environment was exploited in [7, 8], where multipath was utilized to improve detection performance. The potential for exploiting multipath propagation for improved radar detection of moving ground targets in dense urban environments was investigated in [9]. Multipath effects were exploited to both cancel the interference and reinforce the target signal in low grazing angle scenarios [10]. Focusing on the issue of target detection in urban environment, an optimized detection algorithm based on orthogonal frequency division multiplexing (OFDM) radar was proposed in [11, 12]. However, the signal model was idealistic and only considered specular reflections. Based on the same waveform, the problem of target detection in multipath scenarios was reformulated as sparse spectrum estimation [13].

Over the last decades, multi-input multi-output (MIMO) radar system has drawn a large amount of attention due to the different types of diversities. In [14, 15], the authors showed that the statistical MIMO radar provided significant performance improvement compared with other types of array radar. In rich multipath environments, time reversal technique combined with MIMO radar was used to improve the detection performance [16] while a space-time adaptive processing (STAP) method was developed to mitigate the multipath clutter [17, 18]. In [19], the authors demonstrated that the detection

Received 14 December 2015, Accepted 19 January 2016, Scheduled 28 January 2016
* Corresponding author: Yang Xia (xiayang@nudt.edu.cn).
The authors are with the ATR Key Laboratory, National University of Defense Technology, Changsha 410073, P. R. China.

performance could be significantly improved through multipath utilization with statistical MIMO radar. The detection performances of two kinds of generalized likelihood ratio test (GLRT) detectors with hybrid MIMO radar in low grazing angel were discussed in [20].

In this paper, we deal with the problem of target detection in low grazing angle. A colocated MIMO radar configuration is employed with each antenna transmitting one of an OFDM subcarrier frequency. To make the propagation model more accurate, realistic physical and statistical effects are taken into account. A generalized GLRT detector is developed under Gaussian clutter assumption, and an algorithm which adaptively allocates the transmitted energy among different transmitters is proposed to enhance the detection performance. The performances of the GLRT detector are evaluated via numerical examples.

2. MULTIPATH PROPAGATION MODEL

A representative scenario of multipath propagation in low grazing angle is shown in Figure 1. The received signals include not only directly reflected signals but also indirect signals. We consider only the first and second-order reflected signals because signals reflected more than twice can be neglected due to heavy attenuation [9]. The transmitted signal is assumed to be narrow band and denoted by [2]

$$x(t) = be^{j(\omega t+\xi)} \tag{1}$$

where b, ω and ξ denote the amplitude, angular frequency and initial phase, respectively. The direct signal is

$$x_d(t) = x(t)e^{-j2\pi/\lambda R_d}, \tag{2}$$

and the indirect signal is

$$x_i(t) = x(t)\rho e^{j\varphi}e^{-j2\pi/\lambda R_i} \tag{3}$$

In Eqs. (2) and (3), R_d and R_i are the total length of direct and indirect paths, respectively. $\rho e^{j\varphi}$ denotes the complex reflection coefficient which is dependent on the characteristic of the reflected surface. Taking first-order reflected signal for example, the total received signal is

$$r(t) = x_d(t) + x_i(t) = x(t)e^{-j2\pi/\lambda R_d}\left(1 + \rho e^{j\varphi}e^{-j2\pi/\lambda\Delta R}\right) \tag{4}$$

where $\Delta R = R_i - R_d$ and the term $1 + \rho e^{j\varphi}e^{-j2\pi/\lambda\Delta R}$ denotes the multipath propagation factor which is decided by reflection coefficient, wavelength and path difference [5]. It is noted that we will use ρ (a complex value) instead of $\rho e^{j\varphi}$ to represent the complex scattering coefficient hereafter.

To make the signal model more realistic, the curvature of the earth and the signal path due to the refraction in the atmospheric are taken into consideration. The modified multipath propagation model

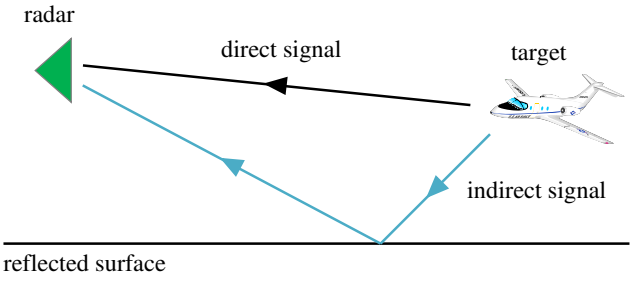

Figure 1. Simple multipath propagation model in flat earth.

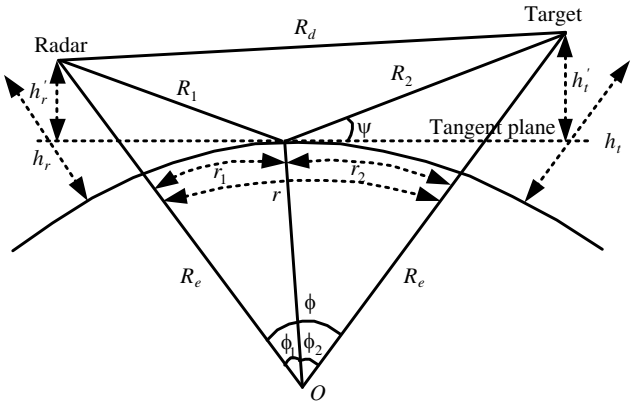

Figure 2. Modified multipath propagation model.

is shown in Figure 2. R_e denotes the effective radius of the imaginary earth and can be represented as [19]

$$R_e = R_0 \left(1 + R_0 \frac{dN}{dh} 10^{-6}\right)^{-1} \tag{5}$$

where R_0 is the radius of actual Earth and dN/dh the refractivity gradient. The grazing angle ψ is calculated by

$$\psi = \frac{1}{2}\left(\pi - \arccos\left(\frac{R_1^2 + R_2^2 - R_d^2}{2R_1R_2}\right)\right) \tag{6}$$

The solutions of other variables (such as r_1, h_r') are omitted for brevity, see [19, 21] for more details.

The complex reflection coefficient is calculated by [22]

$$\rho = \Gamma_{(\nu,h)} DS \tag{7}$$

where $\Gamma_{(\nu,h)}$ is vertical polarization or horizontal polarization reflection coefficient for a plane surface; D is the divergence factor due to a curved surface; S is root-mean-squared (RMS) specular scattering coefficient which represents the roughness of surface.

$\Gamma_{(\nu,h)}$ is determined by frequency, complex dielectric constant and grazing angle ψ and calculated by [22]

$$\Gamma_v \simeq \frac{\sin\psi\sqrt{\varepsilon_c} - 1}{\sin\psi\sqrt{\varepsilon_c} + 1} \tag{8}$$

for vertical polarization and

$$\Gamma_h \simeq \frac{\sin\psi - \sqrt{\varepsilon_c}}{\sin\psi + \sqrt{\varepsilon_c}} \tag{9}$$

for horizontal polarization, where ε_c is complex dielectric constant given by $\varepsilon_c = \varepsilon/\varepsilon_0 - j60\lambda\sigma$. $\varepsilon/\varepsilon_0$ is relative dielectric constant of the reflecting medium, and σ is its conductivity.

The divergence factor D can be approximated by [22]

$$D \simeq \left(1 + \frac{2r_1r_2}{R_e r\psi}\right)^{-1/2} \tag{10}$$

S is related to the grazing angle and the signal wavelength, given by [22]

$$S = e^{-\mu} \tag{11}$$

where

$$\mu = \begin{cases} 2[2\pi\eta]^2 & \eta \le 0.1\,\text{rad} \\ 0.16\eta^2 + 7.42\eta + 0.0468 & \text{otherwise} \end{cases} \tag{12}$$

η is the surface roughness factor defined as $\eta = \sigma_H\psi/\lambda$, σ_H the RMS of reflection surface, and σ_H/λ the roughness of the reflected surface. The larger σ_H/λ is, the rougher the surface will be. For smooth surface, σ_H/λ is approximated to be zero.

Finally, substituting Eqs. (8)–(12) into Eq. (7), we can get complex scattering coefficient ρ.

3. OFDM MIMO RADAR MEASUREMENT MODEL

3.1. OFDM MIMO Radar Signal Model

Consider a colocated MIMO radar with M transmitters and N receivers, where the antennas are configured as uniform linear arrays (ULAs). The MIMO radar signal model is shown in Figure 3, where $\{s_m(t)\}_{m=1}^M$ and $\{r_n(t)\}_{n=1}^N$ denote the transmitted and received signal, respectively. Each transmitted waveform consists of a carrier frequency f_m forming an OFDM signal, which is

$$s_m(t) = a_m e^{j2\pi f_m t}, \quad 0 \le t \le T \tag{13}$$

where $f_m = f_0 + (m-1)\Delta f$. f_0 and Δf represent the carrier frequency and subcarrier spacing, respectively. T denotes the pulse duration of a single pulse. To keep orthogonal between different subcarriers, Δf is the reciprocal of T. a_m is the complex weight corresponding to the m-th subcarrier, which can also be thought as the transmitted energy corresponding to the m-th transmitter. To normalize the total transmitted energy, we have $\sum_{m=1}^M |a_m|^2 = 1$.

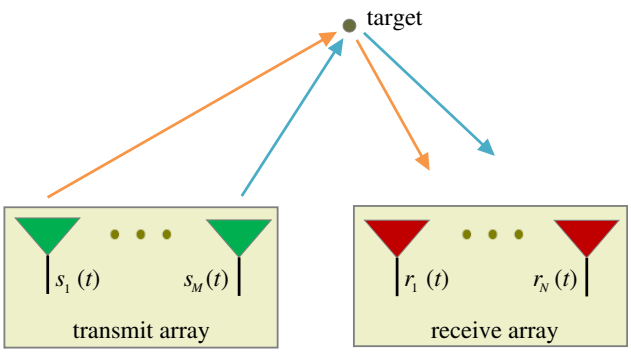

Figure 3. MIMO radar signal model.

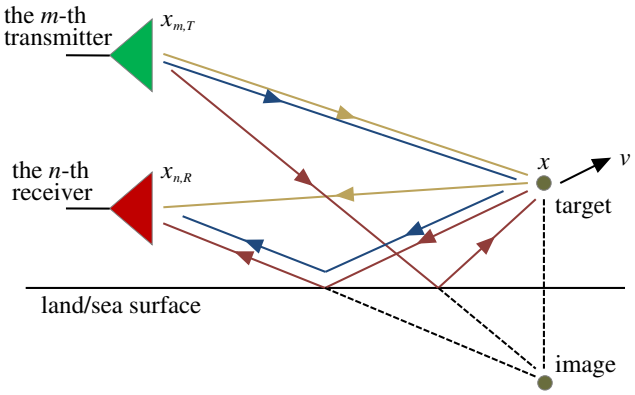

Figure 4. Scenario of multipath propagation in low grazing angle with one transmit-receive channel.

3.2. Measurement Model

Consider a far-field point target located at $\mathbf{x} = (x_0, y_0)^T$ in 2-D Cartesian coordinates with velocity $\mathbf{v}$. The transmitted and received arrays are assumed to be stationary and located at $\mathbf{X}_T = [\mathbf{x}_{1,T}, \mathbf{x}_{2,T}, \ldots, \mathbf{x}_{M,T}]$ and $\mathbf{X}_R = [\mathbf{x}_{1,R}, \mathbf{x}_{2,R}, \ldots, \mathbf{x}_{M,R}]$. Multipath propagation model in low grazing angle scenario is described in Figure 4, where we only give one transmit-receive pair for others are similar. The number of possible propagation paths is P. However, in Figure 4 we only depict three paths with different colors.

The received signal at the n-th receive sensor transmitted by the m-th transmit sensor is

$$y_{mn}(t) = \sum_{p=0}^{P-1} \beta_{m,n}^{p} s_m\left(\gamma_{m,n}^{p}(t - \tau_{m,n}^{p})\right) + e_{m,n}(t) \tag{14}$$

where $\beta_{m,n}^{p}$ denotes the complex scattering coefficient of target along the p-th path of the $(m,\ n)$ transmit-receive pair. For colocated configuration, target scattering coefficients do not change with the aspect angle [23, 24], which means that $\beta_{m,n}^{p}$ does not depend on the positions of transmitters and receivers. Besides, different scattering centers of a target resonate variably at different frequencies [12], and each transmitter radiates a different carrier frequency. Thus, $\beta_{m,n}^{p}$ can be substituted by $\beta_{m,p}$.

Let $\boldsymbol{\beta} = \boldsymbol{\beta}_0 \otimes \boldsymbol{\rho}^T$ be an $M \times P$ matrix with element $\beta_{m,p}$, where $\boldsymbol{\beta}_0 = [\beta_1, \beta_2, \ldots, \beta_M]^T$ and β_m $(m = 1, 2, \ldots, M-1)$ is the scattering coefficient of target at the m-th subcarrier. We assume that the reflection coefficients do not depend on the position of transmit and receive arrays (This is reasonable for colocated configuration with small element space). In other words, $\boldsymbol{\rho} = \boldsymbol{\rho}_{m,n} = [\rho_0, \rho_1, \ldots, \rho_{P-1}]^T$ where ρ_p $(p = 0, 1, \ldots, P-1)$ is the complex reflection coefficient over the p-th path. $e_{m,n}(t)$ represents the clutter and measurement noise along the $(m,\ n)$ transmit-receive channel.

$\tau_{m,n}^{p}$ is the two-way time delay along the p-th path of the $(m,\ n)$ transmit-receive pair. For direct-direct path, $\tau_{m,n} = (||\mathbf{x}_{m,T} - \mathbf{x}|| + ||\mathbf{x}_{n,R} - \mathbf{x}||)/c$; for direct-reflected path, $\tau_{m,n} = (||\mathbf{x}_{m,T} - \mathbf{x}|| + ||\mathbf{x}_{n,R} - \mathbf{x}_{im}||)/c$; for reflected-reflected path, $\tau_{m,n} = (||\mathbf{x}_{m,T} - \mathbf{x}_{im}|| + ||\mathbf{x}_{n,R} - \mathbf{x}_{im}||)/c$. c is the speed of propagation; $||\cdot||$ denotes the Euclidean vector norm; $\mathbf{x}_{im} = (x_0, -y_0)$ is the symmetrical position of target with respect to the land/sea surface.

$\gamma_{m,n}^{p}$ accounts for the stretch factor along the p-th path of the $(m,\ n)$ transmit-receive pair, which is

$$\gamma_{m,n}^{p} = 1 + \frac{f_{m,n}^{p}}{f_0} \tag{15}$$

where $f_{m,n}^{p}$ is the Doppler frequency shift along the p-th path of the $(m,\ n)$ transmit-receive pair. For direct-direct path

$$f_{m,n} = \frac{f_m}{c}\left\langle \frac{\mathbf{x} - \mathbf{x}_{m,T}}{||\mathbf{x} - \mathbf{x}_{m,T}||}, \mathbf{v} \right\rangle + \frac{f_m}{c}\left\langle \frac{\mathbf{x} - \mathbf{x}_{n,R}}{||\mathbf{x} - \mathbf{x}_{n,R}||}, \mathbf{v} \right\rangle \tag{16}$$

for direct-reflected path,

$$f_{m,n} = \frac{f_m}{c}\left\langle \frac{\mathbf{x}-\mathbf{x}_{m,T}}{||\mathbf{x}-\mathbf{x}_{m,T}||}, \mathbf{v} \right\rangle + \frac{f_m}{c}\left\langle \frac{\mathbf{x}-\mathbf{x}_{n,R}^{im}}{||\mathbf{x}-\mathbf{x}_{n,R}^{im}||}, \mathbf{v} \right\rangle \tag{17}$$

for reflected-reflected path,

$$f_{m,n} = \frac{f_m}{c}\left\langle \frac{\mathbf{x}-\mathbf{x}_{m,T}^{im}}{||\mathbf{x}-\mathbf{x}_{m,T}^{im}||}, \mathbf{v} \right\rangle + \frac{f_m}{c}\left\langle \frac{\mathbf{x}-\mathbf{x}_{n,R}^{im}}{||\mathbf{x}-\mathbf{x}_{n,R}^{im}||}, \mathbf{v} \right\rangle \tag{18}$$

where $\mathbf{x}_{m,T}^{im}$ and $\mathbf{x}_{n,R}^{im}$ denote the symmetrical position of the m-th transmitter and the n-th receiver with respect to the land/sea surface, respectively.

Substituting Eqs. (13) and (15) into Eq. (14), the received signal after demodulation is

$$y_{mn}(t) = \sum_{p=0}^{P-1} \beta_{m,p} a_m e^{-j2\pi f_m(1+f_{mn}^p/f_0)\tau_{mn}^p} e^{j2\pi[(m-1)\Delta f + f_m/f_0 f_{mn}^p]t} + e_{mn}(t) \tag{19}$$

We incorporate the information of known range cell (denoted by the round trip delay τ_0) by substituting $t = \tau_0 + kT_r$ $(k = 0, 1, \ldots, K-1)$, where T_r is the pulse repetition interval (PRI) and K the temporal measurements within one coherent processing interval (CPI). Thus, Eq. (19) can be further written as

$$y_{mn}(k) = \sum_{p=0}^{P-1} \beta_{m,p} a_m \phi_{n,m}^p(k, \mathbf{v}) + e_{mn}(k) \tag{20}$$

where

$$\phi_{m,n}^p(k, \mathbf{v}) = e^{-j2\pi f_0 \tau_{mn}^p} e^{j2\pi[(m-1)\Delta f + f_m/f_0 f_{mn}^p](\tau_0 - \tau_{mn}^p + kT_r)} \tag{21}$$

Stacking the measurements into an $NM \times 1$ vector, we obtain a measurement model as follows

$$\mathbf{y}(k) = \mathbf{A}(\mathbf{a})\mathbf{X}\mathbf{\Phi}(k, \mathbf{v}) + \mathbf{e}(k), \quad k = 0, 1, \ldots, K-1 \tag{22}$$

where

- $\mathbf{y}(k) = [\mathbf{y}_1(k)^T, \mathbf{y}_2(k)^T, \ldots, \mathbf{y}_N(k)^T]^T$ is an $NM \times 1$ vector, where $\mathbf{y}_n(k) = [y_{1,n}(k), y_{2,n}(k), \ldots, y_{M,n}(k)]^T$ are the temporal measurements received by the n-th receiver.
- $\mathbf{A}(\mathbf{a}) = \mathbf{I}_N \otimes \mathrm{diag}(\mathbf{a})$ is an $NM \times NM$ complex diagonal matrix. $\mathbf{a} = [a_1, a_2, \ldots, a_M]^T$ represent the transmitted energy distributed among different transmitters and $\otimes$ denotes the Kronecker product.
- $\mathbf{X} = \mathbf{I}_N \otimes \mathrm{blkdiag}(\boldsymbol{\beta}_1^T, \boldsymbol{\beta}_2^T, \ldots, \boldsymbol{\beta}_M^T)$ is an $NM \times NMP$ matrix, where $\boldsymbol{\beta}_m^T$ is the m-th row of $\boldsymbol{\beta}$ denoting the scattering coefficients of target along different paths at m-th subcarrier.
- $\mathbf{\Phi}(k, \mathbf{v}) = [\mathbf{\Phi}_1^T, \mathbf{\Phi}_2^T, \ldots, \mathbf{\Phi}_N^T]^T$ is an $NMP \times 1$ vector containing Doppler information of target over different paths and channels, where $\mathbf{\Phi}_n = [\boldsymbol{\phi}_{1,n}^T, \boldsymbol{\phi}_{2,n}^T, \ldots, \boldsymbol{\phi}_{M,n}^T,]^T$ and $\boldsymbol{\phi}_{m,n}^T = [\phi_{m,n}^0, \phi_{m,n}^1, \ldots, \phi_{m,n}^{P-1}]^T$.
- $\mathbf{e}(k) = [\mathbf{e}_1(k)^T, \mathbf{e}_2(k)^T, \ldots, \mathbf{e}_N(k)^T]^T$ is an $NM \times 1$ vector including the measurement noise, clutter and co-channel interference, where $\mathbf{e}_n(k) = [e_{1,n}(k), e_{2,n}(k), \ldots, e_{M,n}(k)]^T$.

Then, concatenating all the temporal data into an $NM \times K$ matrix, the OFDM MIMO measurement model is

$$\mathbf{Y} = \mathbf{A}(\mathbf{a})\mathbf{X}\mathbf{\Phi}(\mathbf{v}) + \mathbf{E} \tag{23}$$

where $\mathbf{Y} = [\mathbf{y}(0), \mathbf{y}(1), \ldots, \mathbf{y}(K-1)]$ is an $NM \times K$ matrix containing all the temporal data within one CPI; $\mathbf{\Phi}(\mathbf{v}) = [\mathbf{\Phi}(0, \mathbf{v}), \mathbf{\Phi}(1, \mathbf{v}), \ldots, \mathbf{\Phi}(K-1, \mathbf{v})]$ is an $NMP \times K$ matrix containing the Doppler information of target. $\mathbf{E} = [\mathbf{e}(0), \mathbf{e}(1), \ldots, \mathbf{e}(K-1)]$.

3.3. Statistical Model

In this paper, the scattering matrix $\mathbf{X}$ is assumed to be unknown. The measurement noise, clutter and co-channel interference are modeled as temporally white and circularly symmetric zero-mean Gaussian distribution with unknown position definite covariance $\mathbf{C}$. The measurements between different pulses are supposed to be independent. Thus the OFDM MIMO measurements are distributed as

$$\mathbf{Y} \sim \mathcal{CN}_{MN,K}\left(\mathbf{A}(\mathbf{a})\mathbf{X}\mathbf{\Phi}(\mathbf{v}), \mathbf{C} \otimes \mathbf{I}_K\right) \tag{24}$$

4. DETECTION TEST

In this section, we develop a statistical detection test for the OFDM MIMO measurements derived in Section 3. The essence of detection is to decide whether a target is present or not in the range cell under test. Therefore, we construct a decision problem to choose between two possible hypotheses: the null hypothesis $\mathcal{H}_0$ (target-free hypothesis) and the alternate hypothesis $\mathcal{H}_1$ (target-present hypothesis), which can be expressed as

$$\begin{cases} \mathcal{H}_0: \ \mathbf{X} = \mathbf{0}, & \mathbf{C} \text{ unknown} \\ \mathcal{H}_1: \ \mathbf{X} \neq \mathbf{0}, & \mathbf{v}, \mathbf{C} \text{ unknown} \end{cases} \tag{25}$$

According to Eq. (24), the measurements $\mathbf{Y}$ under two hypotheses are distributed as

$$\mathbf{Y} \sim \begin{cases} \mathcal{H}_0: \ \mathcal{CN}_{MN,K}(\mathbf{0}, \mathbf{C} \otimes \mathbf{I}_K) & \mathbf{C} \text{ unknown} \\ \mathcal{H}_1: \ \mathcal{CN}_{MN,K}(\mathbf{A}(\mathbf{a})\mathbf{X}\mathbf{\Phi}(\mathbf{v}), \mathbf{C} \otimes \mathbf{I}_K) & \mathbf{v}, \mathbf{C} \text{ unknown} \end{cases} \tag{26}$$

Theoretically, the Neyman-Pearson (NP) detector is optimal which maximizes the detection probability at a given false alarm rate [25]. However, in our problem the target velocity $\mathbf{v}$ and clutter covariance $\mathbf{C}$ are unknown, and we resort to a GLRT detector, which is suboptimal and replaces the unknown parameters with their maximum likelihood estimates (MLEs). The formulation of GLRT detector is

$$\mathrm{GLR}(\mathbf{v}) = \frac{f\left(\mathbf{Y}|\mathcal{H}_1, \mathbf{v}, \hat{\mathbf{X}}, \hat{\mathbf{C}}_1\right)}{f\left(\mathbf{Y}|\mathcal{H}_0, \hat{\mathbf{C}}_0\right)} \underset{\mathcal{H}_1}{\overset{\mathcal{H}_0}{\lessgtr}} \gamma \tag{27}$$

where γ is the detection threshold decided by the false alarm rate. $\hat{\mathbf{C}}_0$ is the MLE of $\mathbf{C}$ under $\mathcal{H}_0$ while $\hat{\mathbf{X}}$ and $\hat{\mathbf{C}}_1$ are the MLEs of $\mathbf{X}$ and $\mathbf{C}$ under $\mathcal{H}_1$. $f(\mathbf{Y}|\mathcal{H}_0)$ and $f(\mathbf{Y}|\mathcal{H}_1)$ follow a matrix-variate complex Gaussian distribution [26], whose probability density functions (PDFs) are given by

$$f\left(\mathbf{Y}|\mathcal{H}_0\right) = \frac{\exp\left\{-\mathrm{tr}\left(\mathbf{C}^{-1}\mathbf{Y}\mathbf{Y}^H\right)\right\}}{\pi^{MNK}\det(\mathbf{C})^K} \tag{28}$$

and

$$f(\mathbf{Y}|\mathcal{H}_1) = \frac{\exp\left\{-\mathrm{tr}\left[\mathbf{C}^{-1}\left(\mathbf{Y} - \mathbf{A}(\mathbf{a})\mathbf{X}\mathbf{\Phi}(\mathbf{v})\right)\left(\mathbf{Y} - \mathbf{A}(\mathbf{a})\mathbf{X}\mathbf{\Phi}(\mathbf{v})\right)^H\right]\right\}}{\pi^{MNK}\det(\mathbf{C})^K} \tag{29}$$

respectively.

The log-likelihood function of Eq. (28) is

$$\ln f(\mathbf{Y}|\mathcal{H}_0) = -MNK\ln\pi - K\ln\det(\mathbf{C}) - \mathrm{tr}\left(\mathbf{C}^{-1}\mathbf{Y}\mathbf{Y}^H\right) \tag{30}$$

Taking derivative of Eq. (30) with respect to $\mathbf{C}$ and making it equal to zero, we get the MLE of $\mathbf{C}$ under $\mathcal{H}_0$

$$\hat{\mathbf{C}}_0 = \frac{1}{K}\mathbf{Y}\mathbf{Y}^H \tag{31}$$

Similarly, the log-likelihood function of Eq. (29) is

$$\ln f(\mathbf{Y}|\mathcal{H}_1) = -MNK\ln\pi - K\ln\det(\mathbf{C}) - \mathrm{tr}\left[\mathbf{C}^{-1}\left(\mathbf{Y} - \mathbf{A}(\mathbf{a})\mathbf{X}\mathbf{\Phi}(\mathbf{v})\right)\left(\mathbf{Y} - \mathbf{A}(\mathbf{a})\mathbf{X}\mathbf{\Phi}(\mathbf{v})\right)^H\right] \tag{32}$$

Taking derivative of Eq. (32) with respect to $\mathbf{C}$ and making it equal to zero, we get the MLE of $\mathbf{C}$ under $\mathcal{H}_1$

$$\hat{\mathbf{C}}_1 = \frac{1}{K}\left(\mathbf{Y} - \mathbf{A}(\mathbf{a})\mathbf{X}\mathbf{\Phi}(\mathbf{v})\right)\left(\mathbf{Y} - \mathbf{A}(\mathbf{a})\mathbf{X}\mathbf{\Phi}(\mathbf{v})\right)^H \tag{33}$$

In our problem, the scattering matrix is also unknown. Substituting Eq. (33) into Eq. (32), the ML estimator of $\mathbf{X}$ can be formulated as

$$\hat{\mathbf{X}}_{\mathrm{ML}} = \arg\min_X \ln\left|\left(\mathbf{Y} - \mathbf{A}(\mathbf{a})\mathbf{X}\mathbf{\Phi}(\mathbf{v})\right)\left(\mathbf{Y} - \mathbf{A}(\mathbf{a})\mathbf{X}\mathbf{\Phi}(\mathbf{v})\right)^H\right| \tag{34}$$

However, the MLE of $\mathbf{X}$ does not yield a closed-form due to the block-diagonal structure. Noting that the measurement model is referred to as the block-diagonal growth curve (BDGC) model [27], an approximate ML (AML) estimator of $\mathbf{X}$ is developed in [27, 28]. We omit the detailed derivation of $\hat{\mathbf{X}}_{\mathrm{ML}}$ for brevity, see [12, 27, 29] for more details.

Then, substituting the estimator $\hat{\mathbf{C}}_0$ under $\mathcal{H}_0$ into Eq. (28), the likelihood function under $\mathcal{H}_0$ is

$$f(\mathbf{Y}|\mathcal{H}_0) = \frac{\exp(-KMN)}{\pi^{MNK}|\hat{\mathbf{C}}_0|^K} \tag{35}$$

Similarly, substituting the estimator $\hat{\mathbf{C}}_1$ under $\mathcal{H}_1$ into Eq. (29), the likelihood function under $\mathcal{H}_1$ is

$$f(\mathbf{Y}|\mathcal{H}_1) = \frac{\exp(-KMN)}{\pi^{MNK}|\hat{\mathbf{C}}_1|^K} \tag{36}$$

Finally, substituting Eqs. (35), (36) into Eq. (27) and after some algebraic manipulations, we come up with the following test statistic

$$\mathrm{GLR}(\mathbf{v}) = \frac{|\hat{\mathbf{C}}_0|}{|\hat{\mathbf{C}}_1|} = \frac{\left|(1/K)\mathbf{Y}\mathbf{Y}^H\right|}{\left|(1/K)\left(\mathbf{Y} - \mathbf{A}(\mathbf{a})\hat{\mathbf{X}}\mathbf{\Phi}(\mathbf{v})\right)\left(\mathbf{Y} - \mathbf{A}(\mathbf{a})\hat{\mathbf{X}}\mathbf{\Phi}(\mathbf{v})\right)^H\right|} \tag{37}$$

Since the target velocity $\mathbf{v}$ is unknown, the GLRT detector turns to be $\max_{\mathbf{v}} \mathrm{GLR}(\mathbf{v}) = \mathrm{GLR}(\hat{\mathbf{v}})$, which is compared with a threshold.

5. ADAPTIVE DESIGN

In this section, we develop an algorithm which adaptively allocates the transmitted energy among different transmitters to enhance the detection performance. Based on the fact that the target responses resonate at different frequencies, which is equivalent to say that target scattering coefficients vary at different transmitters in OFDM MIMO radar, the transmitted energy can be optimally distributed. First, we derive the asymptotic statistical characteristic of the detection test derived in Section 4. Then, an optimal algorithm is proposed to improve the detection performance.

Under $\mathcal{H}_0$ hypothesis, the measurement is distributed as $\mathbf{Y} \sim \mathbb{C}\mathcal{N}_{MN,K}(\mathbf{0}, \mathbf{C} \otimes \mathbf{I}_K)$. Following a similar approach in [26, 30], we find that $1/\mathrm{GLR}(\mathbf{v})$ is the product of a set of independent complex central beta variables, which is similar to Wilk's Lamda statistic in the case of real data. In [31] the authors derived the asymptotic expansion of three statistics under the framework of generalized multivariate analysis of variance (GMANOVA). Similarly, in [Ch. 8, 32] the authors also derived the asymptotic expansion of the distribution of the likelihood ratio criterion. Therefore, following the results in [31–33], we know that $K \ln \mathrm{GLR}(\mathbf{v})$ has a complex chi-square distribution with MN degrees of freedom when $K \to \infty$, which is $K \ln \mathrm{GLR}(\mathbf{v}) \sim \mathbb{C}\chi^2_{MN}$. Since this distribution does not depend on clutter covariance, the test statistic tends to a constant false-alarm rate (CFAR) test when $K \to \infty$.

Similarly, under $\mathcal{H}_1$ hypothesis $K \ln \mathrm{GLR}(\mathbf{v})$ has a noncentral complex chi-square distribution with MN degrees of freedom when $K \to \infty$, which is $K \ln \mathrm{GLR}(\mathbf{v}) \sim \mathbb{C}\chi^2_{MN}(\lambda)$. The noncentral parameter is

$$\lambda = \mathrm{tr}\left(\mathbf{C}^{-1}\left(\mathbf{A}(\mathbf{a})\mathbf{X}\mathbf{\Phi}(\mathbf{v})\right)\left(\mathbf{A}(\mathbf{a})\mathbf{X}\mathbf{\Phi}(\mathbf{v})\right)^H\right) \tag{38}$$

According to [30], the detection performance is proportional to the noncentral parameter λ. Therefore, the detection performance can be improved through maximizing the noncentral parameter. The optimization problem can be formulated as

$$\mathbf{a}_{\text{opt}} = \arg\max_{\mathbf{a}} \left\{ \text{tr}\left(\mathbf{C}^{-1} \left(\mathbf{A}(\mathbf{a})\mathbf{X}\mathbf{\Phi}(\mathbf{v}) \right) \left(\mathbf{A}(\mathbf{a})\mathbf{X}\mathbf{\Phi}(\mathbf{v}) \right)^H \right) \right\} \quad \text{subject to } \mathbf{a}^H\mathbf{a} = 1 \tag{39}$$

where $\mathbf{a}^H\mathbf{a} = 1$ is the transmitted energy constraint. A non-optimal $\mathbf{a}$ will be transmitted in the first K pulses. Then we estimate $\hat{\mathbf{v}}$ and $\hat{\mathbf{X}}$ through $\max_{\mathbf{v}} \text{GLR}(\mathbf{v}) = \text{GLR}(\hat{\mathbf{v}})$ and (34) respectively. The clutter covariance is estimated by $\hat{\mathbf{C}} = 1/K(\mathbf{Y} - \mathbf{A}(\mathbf{a})\hat{\mathbf{X}}\mathbf{\Phi}(\hat{\mathbf{v}}))(\mathbf{Y} - \mathbf{A}(\mathbf{a})\hat{\mathbf{X}}\mathbf{\Phi}(\hat{\mathbf{v}}))^H$. Finally the optimal $\mathbf{a}_{\text{opt}}$ is calculated though solving Eq. (39).

6. NUMERICAL RESULTS

In this section, we present several numerical examples to illustrate performances of the proposed detector. We consider a special case of MIMO radar, where the transmit array is also the receive array ($M = N$). The simulation scenario is described in Figure 2, and the simulation parameters are shown in Table 1. Since the closed-form expression of false alarm rate and threshold is not available, we use Monte Carlo simulations instead. We assume that the entries of $\mathbf{C}^{-1/2}$ are generated from $C\mathcal{N}(0,1)$ distribution and then are scaled to satisfy the required SCR. The definition of signal to clutter (SCR) is similar to [34], which is

$$\text{SCR} = \frac{1}{K} \frac{\sum_{k=1}^{K} \left(\mathbf{A}(\mathbf{a})\mathbf{X}\mathbf{\Phi}(k,\mathbf{v}) \right)^H \left(\mathbf{A}(\mathbf{a})\mathbf{X}\mathbf{\Phi}(k,\mathbf{v}) \right)}{\text{tr}(\mathbf{C})} \tag{40}$$

Table 1. Parameter settings of the simulations.

Parameters	Values
Carrier frequency f_0	1 GHz
Bandwidth B	100 MHz
Frequency weights $\mathbf{a}$	$1/\sqrt{M}\mathbf{I}_M$
Pulse repetition interval T_r	2 ms
Pulse number K	40
Height of the radar platform	200 m
Height of target	100 m
Relative distance between radar and target	5 km
Scattering coefficient of the target $\mathbf{X}$	$\mathbb{C}\mathcal{N}(0,1)$
Multipath number P	3
signal to clutter (SCR)	-25 dB

In Figure 5, we show the receiver operating characteristics (ROC) curves with different transmitters and receivers, where the number of transmit and receive antennas is $N = M = 2$, 3, 4, respectively. If not explicit stated, other parameters are the same as in Table 1. As expected, the detection performance is improved with increasing the antenna number. We exploit the target response at different frequencies as well as the frequency diversity among different transmit antennas due to the OFDM MIMO radar scheme to improve the detection performances.

The effects of multipath number on the detection performances at different SCRs are shown in Figure 6, where the number of transmit and receive antennas is $N = M = 3$. Here, $P = 1$ means that we only consider the line of sight (LOS) return. The curves show that the detection performance can be improved through exploiting the multipath effect with OFDM MIMO radar. At the same time, the results also show that the detection performance is improved as SCR is increased.

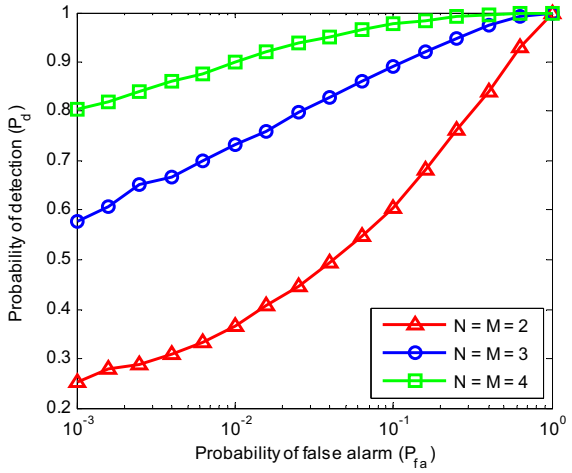

Figure 5. Detection performances with different transmitters and receivers.

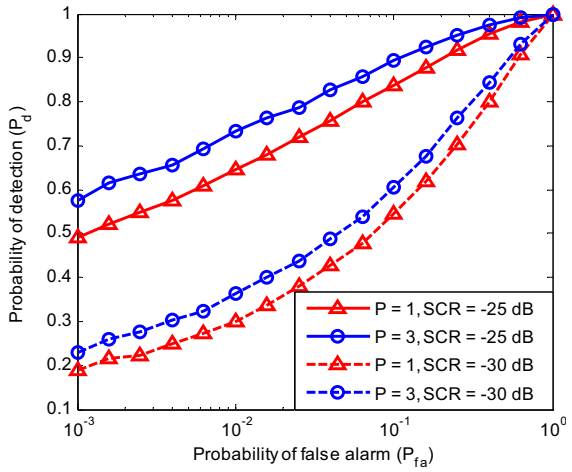

Figure 6. Detection performances with different path numbers and SCRs.

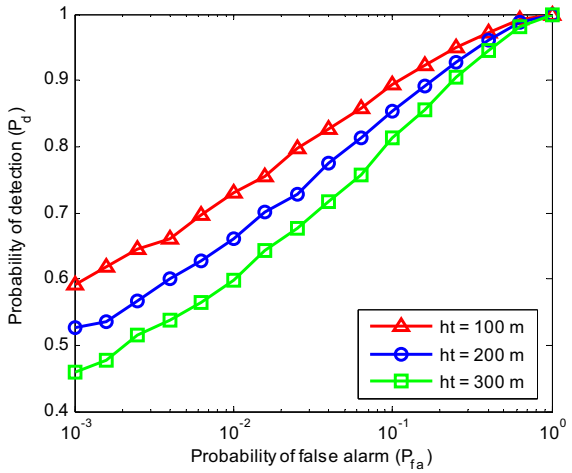

Figure 7. Detection performances with different target heights.

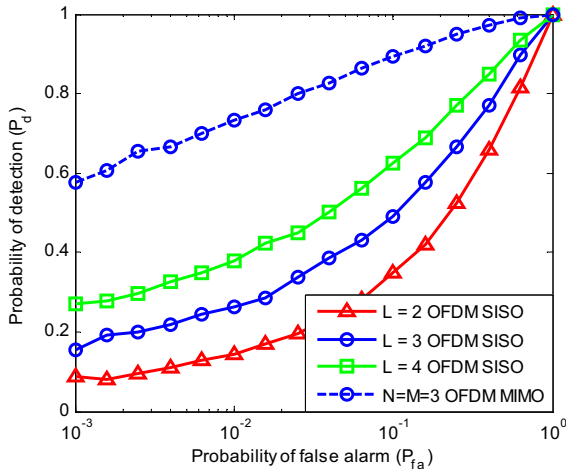

Figure 8. Comparison of detection performances between monostatic OFDM and OFDM MIMO radar.

Figure 7 depicts the detection performances with different target heights, where the transmit and receive antennas are $N = M = 3$. The results show that the detection performance decreases with the increase of target height in low grazing angle scenario. As the target height becomes larger, the grazing angle gets larger, and the complex scattering coefficient becomes smaller. Therefore, the detection performances decrease.

We compare performances of the detector with that in [12] which was derived with OFDM single-input single-output (SISO) radar. The results are shown in Figure 8, where L denotes the subcarrier number in OFDM SISO radar system. As for OFDM SISO radar, the detection performance is improved with increasing the subcarrier number, which agrees with the conclusions in [12]. However, the detection performances of OFDM MIMO with $N = M = 3$ (which means that three subcarriers are used) outperform that of the OFDM SISO radar with $L = 2$, 3, 4, because the measurements of OFDM MIMO radar are more than that of OFDM SISO radar, and more information can be obtained. The results confirm the advantages of using MIMO radar.

Finally, we compare the adaptive design method with that distributing energy equally among different transmitters. We assume that the transmitted waveform in the first K pulses has equal weights,

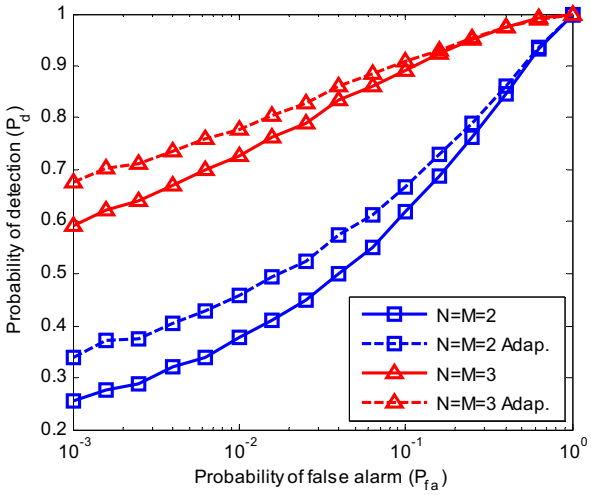

Figure 9. Detection performances with and without adaptive energy allocation.

i.e., $1/\sqrt{M}\mathbf{I}_M$. Then based on Eq. (39), we compute $\mathbf{a}_{\text{opt}}$ for the next K pulses. We show the detection performance improvement due to the adaptively energy allocation in Figure 9. Since the target RCS varies among different subcarriers, the transmitted energy can be optimally allocated accordingly.

7. CONCLUSIONS

In this paper, we address the problem of target detection in low grazing angle with OFDM MIMO radar. To make the propagation model more accurate, we incorporate the realistic physical and statistical effects. Based on the characteristic of OFDM MIMO radar system and the multipath propagation model, we develop an OFDM MIMO measurement model and derive a GLRT detector under Gaussian clutter assumption. Then we propose an adaptive design algorithm based on maximizing the noncentral parameter of the distribution of test statistical to enhance the detection performance. We show that the detection performances are improved due to the multipath utilization as well as the adaptive design method. We also demonstrate that the detection performances of OFDM MIMO radar outperform the monostatic OFDM radar. However, we only consider Gaussian clutter assumption, and we will extend our work to more general situations such as compound Gaussian clutter in the future work.

8. DISCLOSURE STATEMENT

No potential conflict of interest was reported by the authors.

ACKNOWLEDGMENT

The authors wish to thank the anonymous reviewers for their efforts in providing comments that have helped to significantly enhance the quality of this paper. This work was supported in part by the National Natural Science Foundation of China under Grant No. 61401475.

REFERENCES

1. Barton, D., "Low-angle radar tracking," *Proc. of the IEEE*, Vol. 62, No. 6, 210–225, 1974.
2. Lo, T. and J. Litva, "Use of a highly deterministic multipath signal model in low-angle tracking," *IEE Proc. F — Radar and Signal Processing*, Vol. 138, No. 2, 163–171, 1991.

3. Chakraborty, B., Y. Li, J. J. Zhang, et al., "Multipath exploitation with adaptive waveform design for tracking in urban terrain," *Proceedings of the IEEE Acoustics Speech and Signal Processing (ICASSP)*, 3894–3897, Dallas, TX, United States, 2010.
4. Silon, S. L. and B. D. Carlson, "Radar detection in multipath," *IEE Proc. Radar, Sonar and Navigation*, Vol. 146, No. 1, 45–54, 1999.
5. Zhao, J. H. and J. Y. Yang, "Frequency diversity to low-angle detecting using a highly deterministic multipath signal model," *Proc. of 6th CIE Int. on Radar*, 1–5, Shanghai, China, 2006.
6. Ge, P., L. J. Kong, and J. Y. Yang, "Moving target detection with frequency diversity under multipath scenario," *Proceedings of 2014 IEEE International Conference on Communication Problem-Solving (ICCP)*, 197–201, Beijing, China, 2014.
7. Hayvaci, H. T., A. de Maio, and Erricolo, "Improved detection probability of a radar target in the presence of multipath with prior knowledge of the environment," *IET Radar, Sonar & Navigation*, Vol. 7, No. 1, 36–46, 2013.
8. Hayvaci, H. T. and D. Erricolo, "Improved radar target time-delay estimation with multipath exploitation," *Proceedings of the 2013 International Conference on Electromagnetics in Advanced Applications (ICEAA)*, 1232–1235, Turin, Italy, 2013.
9. Krolik, J. L., J. Farrell, and A. Steinhardt, "Exploiting multipath propagation for GMTI in urban environments," *Proceedings of 2006 IEEE Radar Conference*, 65–68, Verona, NY, United States, 2006.
10. Paul, E. B. and D. P. Finch, "Low-angle target detection with interference in a multipath environment," *Proceedings of 2013 International Conference on Radar*, 440–445, Adelaide, SA, Australia, 2013.
11. Sen, S., M. Hurtado, and A. Nehorai, "Adaptive OFDM radar for detecting a moving target in urban scenarios," *Proceedings of 2009 International Waveform Diversity and Design (WDD) Conference*, 268–272, Orlando, USA, 2009.
12. Sen, S. and A. Nehorai, "Adaptive OFDM radar for target detection in multipath scenarios," *IEEE Trans. on Signal Processing*, Vol. 59, No. 1, 78–90, 2011.
13. Sen, S., G. Tang, and A. Nehorai, "Multi-objective optimization of OFDM radar waveform for target detection," *IEEE Trans. on Signal Processing*, Vol. 59, No. 2, 639–652, 2011.
14. Fisher, E., A. Haimovich, R. Blum, et al., "MIMO radar: An idea whose time has come," *Proceedings of the 2004 IEEE Radar Conference*, 71–78, Philadelphia, Pennsylvania, 2004.
15. Fishler, E., A. Haimovich, and R. Blum, "Spatial diversity in radars-models and detection performance," *IEEE Trans. on Signal Processing*, Vol. 54, No. 3, 823–838, 2006.
16. Jin, Y., J. M. F. Moura, and N. O. Donoughue, "Time reversal in multiple-input multiple-output radar," *IEEE Journal of Selected Topics in Signal Processing*, Vol. 4, No. 1, 210–225, 2010.
17. Mecca, V. F., D. Ramakrishnan, and J. L. Krolik, "MIMO radar space-time adaptive processing for multipath clutter mitigation," *Proceedings of 4th IEEE Sensor Array and Multichannel Signal Processing Workshop*, 249–253, Waltham, MA, United States, 2006.
18. Tohidur Rahman, A. K. M., S. M. M. Hossain Mahmud, and T. K. Biswas, "Target detection performance of coherent MIMO radar using space time adaptive processing," *Proceedings of 3rd International Conference on Informatics, Electronics & Vision (ICIEV)*, 1–5, Dhaka, Bangladesh, 2014.
19. Ding, J., H. W. Chen, H. Wang, X. Li, and Z. Zhuang, "Low-grazing angle target detection and system configuration of MIMO radar," *Progress In Electromagnetics Research B*, Vol. 48, 23–42, 2013.
20. Ding, J. C., H. W. Chen, H. Q. Wang, et al., "Low-grazing angle detection in compound-Gaussian clutter with hybrid MIMO radar," *International Journal of Antennas and Propagation*, Vol. 2013, Article ID374342, 2013.
21. Bar-Shalom, Y., A. Kumar, W. Blair, and G. Groves, "Tracking low elevation targets in the presence of multipath propagation," *IEEE Trans. on Aerospace and Electronic Systems*, Vol. 30, No. 3, 973–979, 1994.

22. Long, M. W., *Radar Reflectivity of Land Sea*, 3rd Edition, Artech House, Apr. 2001.
23. Jian, L. and P. Stoica, "MIMO radar with colocated antennas," *IEEE Trans. on Signal Processing Magazine*, Vol. 24, No. 5, 106–114, 2007.
24. Michael, S. D., A. S. Gregory, and A. Lanterman, "Coherent MIMO radar: The phased array and orthogonal waveforms," *IEEE Trans. on Aerospace and Electronic Systems Magazine*, Vol. 29, No. 8, 76–91, 2014.
25. Kay, S. M., *Fundamentals of Statistical Signal Processing: Detection Theory*, Prentice Hall PTR, Upper Saddle River, NJ, 1998.
26. Andersen, H. H., M. Højbjerre, D. Sørensen, and P. S. Eriksen, *Linear and Graphical Models for Multivariate Complex Normal Distribution*, Springer-Verlag, Inc., New York, NY, 1995.
27. Xu, L., P. Stoica, and J. Li, "A block-diagonal growth curve model," *Digital Signal Process.*, Vol. 16, No. 6, 902–912, 2006.
28. Xu, L., P. Stoica, and J. Li, "A diagonal growth curve model and some signal processing applications," *IEEE Trans. on Signal Processing*, Vol. 54, No. 9, 3363–3371, 2006.
29. Dogandzic, A. and A. Nehorai, "Generalized multivariate analysis of variance: A unified framework for signal processing in correlated noise," *IEEE Trans. on Signal Processing Magazine*, Vol. 20, 39–54, 2003.
30. Kelly, E. J. and K. M. Forsythe, "Adaptive detection and parameter estimation for multidimensional signal models," Tech. Rep. 848, Lincoln Laboratory, MIT, Lexington, MA, Apr. 1989.
31. Fujikoshi, Y., "Asymptotic expansions of the non-null distributions of three statistics in GMANOVA," *Annals of the Institute of Statistical Mathematics*, Vol. 26, No. 1, 289–297, 1974.
32. Anderson, T. W., *An Introduction to Multivariate Statistical Analysis*, 2nd Edition, Wiley, Hoboken, NJ, Sep. 2003.
33. Bickel, P. and K. Doksum, *Mathematical Statistics: Basic Ideas and Selected Topics*, 2nd Edition, Prentice-Hall, Upper Saddle River, NJ, 2000.
34. Akcakaya, M. and A. Nehorai, "Adaptive MIMO radar design and detection in compound-Gaussian clutter," *IEEE Trans. on Aerospace and Electronic Systems*, Vol. 47, No. 3, 2200–2207, 2011.